Characterization and Photocatalytic Evaluation (UV-Visible) of Fe-doped TiO_2 Systems Calcined at Different Temperatures

Ximena María Vargas*,[1], Juan Miguel Marin[2], Gloria Restrepo[2]

[1]Facultad de Ingeniería, Universidad del Atlántico, Km 7 antigua vía a Puerto Colombia, Barranquilla, Colombia
[2]Grupo Procesos Fisicoquímicos Aplicados, Departamento de Ingeniería Química, Facultad de Ingeniería, Universidad de Antioquia UdeA; calle 70 No. 52-21 Medellín, Colombia

Abstract:

There is growing interest in obtaining compounds with photocatalytic activity in the solar spectrum, and this has led to intense research on the topic. In our laboratory, Fe-doped TiO_2 was synthesized using the sol-gel method combined with the solvothermal technique at 200°C and calcined at temperatures between 350°C and 620°C. The samples were characterized by X-ray diffraction, Micro-Raman spectroscopy, Brunauer-Emmett-Teller specific surface area, diffuse reflectance spectroscopy, X-ray fluorescence and photocatalytic activity. All materials crystallized in the anatase phase. Additionally the 0.05% Fe-doped TiO_2 calcined at 620°C showed the presence of the rutile phase while 0.1% Fe-doped TiO_2 calcined at 620°C showed the presence of the brookite phase. Photoactivity was observed in the visible spectrum for 0.05% and 0.1% Fe-doped TiO_2, calcined at 620°C. Visible activity was attributed to the presence of rutile and an absorption shift to the visible spectrum. Because of the temperature increment, the crystal size grew and the surface area decreased.

Keywords: heterogeneous photocatalysis, TiO_2, iron doping, visible spectrum.

Introduction

Industrial development has led to the environmental degradation of water resources throughout the world, which has caused the proliferation of health problems and water-related diseases. Moreover, climate change has caused huge hydrological changes, such as an increase in water temperature and the growth of pollution loads (chemical and microbiological) (1). To counteract some of these effects, additional treatments are needed, as is a more effective way to remove pollutants. Nanotechnology offers the potential to treat surface water, groundwater, and wastewater that has been contaminated with toxic metal ions, microorganisms, and organic and inorganic substances with novel nanomaterials. Due to its unique activity towards persistent compounds and the flexibility in their application, many nanomaterials are the subject of extensive research and development (2).

Among the most versatile materials used in nanotechnology is titanium dioxide (TiO_2), a powerful promotor of oxidizing agents (3-4). When TiO_2 is exposed to UV radiation, it is able to break down the molecules that make up pesticides, dyes, and acids, as well as other compounds (5-7). However, it has a low potential to act under the visible spectrum and its rapid electron-hole recombination decreases its activity. In the last decade, scientists have been testing innovations in heterogeneous photocatalysis aimed to at increasing the photocatalytic activity, reducing the electron-hole recombination, and enhancing the augmentation of TiO_2 absorption into the visible spectrum in order to take advantage of a greater percentage of incident solar radiation on the surface of the Earth (because TiO_2 only absorbs approximately 5% of the spectrum in terms of energy at ground level) (8). Doping TiO_2 with transition metals (such as iron) has been proposed. Iron (Fe) has the ability to fit easily into the crystal structure of titanium due to its similar atomic radius, and Fe^{3+} ions can act as both hole and electron traps that improve the photocatalytic activity of TiO_2 (9). In addition, iron is locally available, has a low cost and recent studies have shown good performance for iron doping under solar irradiation compared to other doping metals (10). This paper discusses Fe-doped TiO_2 nanoparticles synthesized by the sol-gel method coupled with the solvothermal technique at 200°C, evaluating different calcination temperatures (350°C-620°C). We selected these temperatures based on recent publications that have reported activity in the visible spectrum, using Fe-doping TiO_2 calcined at temperatures between 500°C and 700°C (9, 11). Despite the various studies that have been conducted, there is little clarity about which factors affect the

*Corresponding author;
E-mail address: ximenavargas@mail.uniatlantico.edu.co

visible photoactivity for iron-doped TiO_2. There are different optimal iron doped concentrations reported in the literature (12-17), and these depend on the synthesis method. After a literature review, we selected different amounts of iron for doping titanium (some of which were presented in a previous work (18)), that allowed us to define the percentages of iron for this study to evaluate the calcination at different temperatures. The Fe-doped TiO_2 synthesis used two different iron contents (Fe:Ti molar ratio percentage = 0.05% and 0.1%). The photoactivity in the ultraviolet and visible spectra was determined in the degradation of the commercial and non-biodegradable dye Cibacron Yellow LS-R, which is commonly used in the dyeing of cotton fabric (19) and phenol.

Materials and Methods

Reagents

The following materials were used in the synthesis: tetraisopropyl orthotitanate ($Ti(OC_3H_7)_4$), 98% isopropyl alcohol ($(CH_3)_2CHOH$, 99.8%), hydrochloric acid (HCl), 37%, ferric nitrate nonahydrate ($Fe(NO_3)_3$. $9H_2O$) , 99%), and Milli Q water. All reagents were obtained from Merck. As model substances, we used Cibacron Yellow LS-R ($C_{45}H_{38}O_{14}N_{16}S_4F_2$) provided by Hunstmann, and 99% phenol from Merck. Degussa P-25 (DP-25) from Evonik was used as a commercial photocatalyst.

Catalyst Synthesis

Fe-doped TiO_2 samples were prepared via the sol-gel method combined with the solvothermal technique by mixing 11.40 mL of isopropyl alcohol with 8.87 mL of tetraisopropyl orthotitanate, followed by the addition of 0.54 mL of water containing $Fe(NO_3)_3$. $9H_2O$ (Fe:Ti molar ratio percentage = 0.05% and 0.1 %). After 2 h of continuous stirring, 0.15 mL of HCl (3 mol L^{-1}) was added, and the solution was heated at 200˚C in a stainless steel-Teflon autoclave for 2 h. The samples were then filtered through a 0.45-µm filter and rinsed with isopropyl alcohol. After cooling to ambient temperature, the product was separated, dried at 100°C, and ground. Finally, the samples were calcined at temperatures of 350˚C, 500°C and 620˚C for 4 hours, under atmospheric air. The materials were named using first the letter s, followed by the iron percentage (0.05% and 0.1%) and finally the treatment temperature (200˚C, 350˚C, 500˚C and 620˚C).

Characterization

For X-ray diffraction (XRD), a Rigaku Minifles diffractometer (Cu-Kα radiation with 2θ from 0˚ to 70˚ at a scan rate of 2°/minute) was used. The average crystallite size of anatase was estimated according to the Scherrer equation (20), using the full-width at half-maximum (FWHM) of the peak corresponding to the (101) reflection. UV-Vis Diffuse Reflectance spectra (DRS) were obtained using an Evolution 600 UV-Vis spectrophotometer from Thermo Electron Corporation, with an attenuated diffuse-reflectance sphere and a Labsphere spectralon as a reference. The Brunauer-Emmett-Teller (BET) specific surface area was determined using a Gemini V Micromerities with nitrogen gas as the adsorbate at 77 K. The doped samples were degassed for one hour and purged with nitrogen at 150˚C for two hours. For the Raman analysis, we used a Horiba Jobin Yvon Lab RAM HR 800 Microraman. Elemental analysis of the samples was carried out using at an "Eagle II" X-ray fluorescence (XRF) system with micro focus (energy dispersive, Roentgenanalytik GmbH, Rh tube, Si(Li) detector, 50 µm spot size).

The UV photocatalytic activity measurements were carried out in borosilicate glass reactors with a 200 mL capacity, with lamps located at 15 cm from the reactor and with an average UV irradiance of 27 W/m^2 and permanent aeration. As model substances, a 60 mg/L solution of Cibacron Yellow LS-R (pH of 6.5) and 50 mg/L of phenol were prepared, and a catalyst dose of 200 mg/L was used. Photolysis tests were performed during the same period of degradation, in addition to the adsorption tests. Adsorption equilibrium was achieved after an hour. An initial sample was taken after reaching the adsorption equilibrium. Another sample was taken after 4 hours of irradiation. For the tests under the visible spectrum, we used Electroxx PAR 38 lamps with a power of 20 W. The degradation time was increased up to 6 hours; we also degraded phenol, which was evaluated under the same conditions as the dye. The concentrations of the dye were measured with a Thermo Evolution 600 UV-Vis spectrophotometer at 400 nm. For phenol, we performed HPLC using Hitachi D-7000 (LaChrom) equipment through an L-7200 auto sampler, and also using a Lichrosphere 60 Select B column, a UV-VIS L-7400 as the absorbance detector and a mixture of water, sulfuric acid and methanol as the mobile phase. We used different lamps for the UV and visible light. The maximum UV emission was at a wavelength of 366 nm, and for visible light, at approximately 580 nm. We also used a filter to avoid UV radiation during visible-light photodegradation.

Results and Discussion

X-ray Powder Diffraction (XRD) Analysis

Figure 1 shows the XRD diffractograms of the TiO_2 samples doped with 0%, 0.05% and 0.1% iron

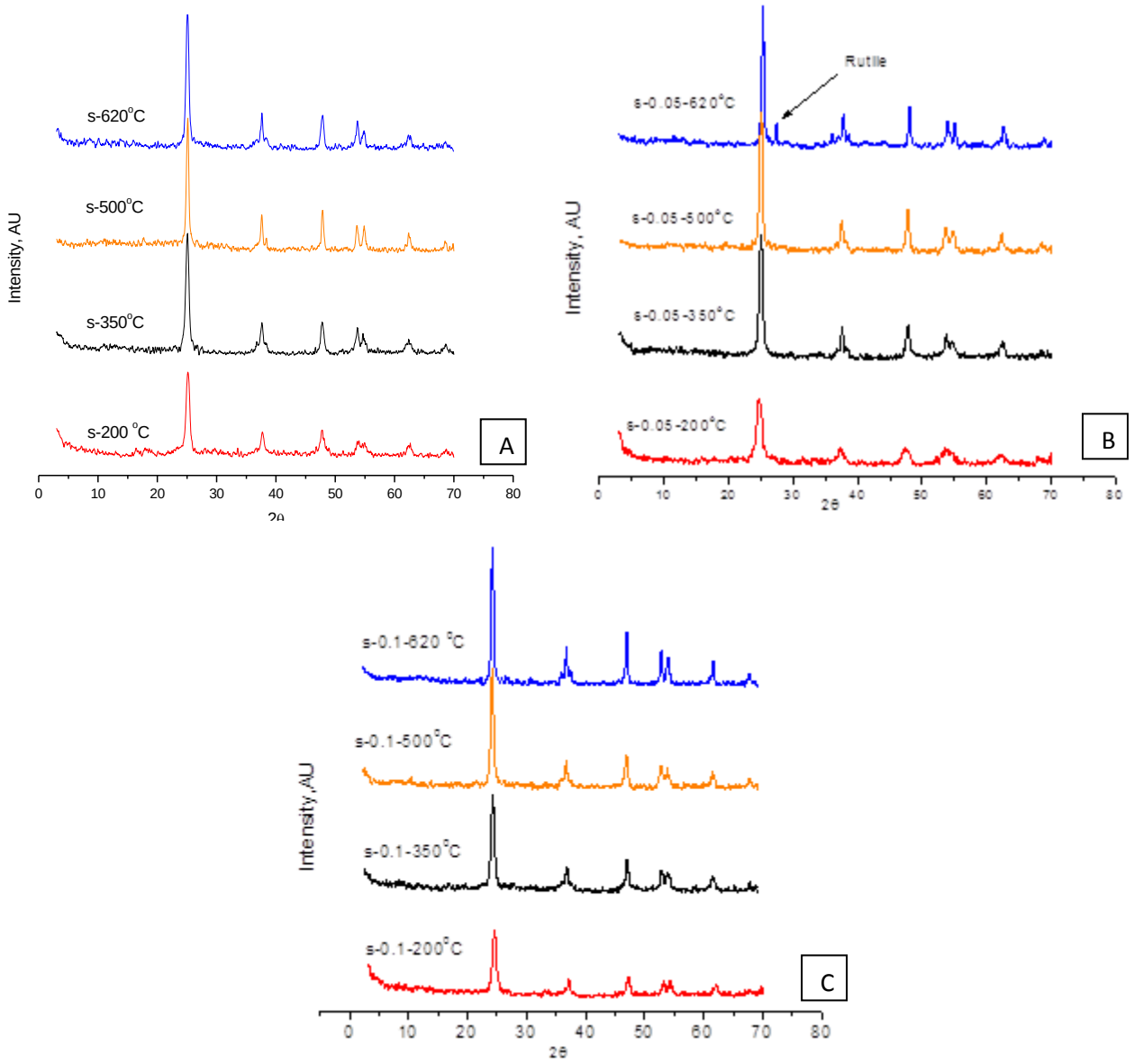

Figure 1. Diffractograms for a) undoped TiO_2, b) 0.05% Fe-doped TiO_2 and c) 0.1% Fe-doped TiO_2, without calcination (200°C) and calcined at 350°C, 500°C and 620°C.

molar percentage at 200°C (without calcination) and calcined at 350°C, 500°C and 620°C. The rutile phase fraction was calculated according to Equation 1 (21).

$$F_R = \frac{1}{1 + 0{,}79\left(\frac{I_{A101}}{I_{R110}}\right)} \qquad \text{Eq. 1}$$

where I_{A101} and I_{R110} are the intensities of the main anatase and rutile peaks, respectively.

The synthesized materials were crystallized in pure anatase except the 0.05% Fe-doped TiO_2 calcined at 620°C, which showed the presence of the rutile phase. The presence of the anatase phase was verified with the patterns of X-ray diffraction (file PDF # 21-1272) with some of the major peaks at 2θ values of 25.281°, 36.94°, 48.050°, 55.062° and 62.69°, corresponding to the spacings of (101), (004), (200), (211) and (204) planes, respectively. These patterns were compared and matched with the respective diffractograms.

The absence of other phases in the doped samples at lower temperatures is attributed to the fact that Fe^{3+} ions can replace the Ti^{4+} ions when inserted into the crystal structure, and the radii of these ions—with coordination number 6—are similar: 0.79 Å and 0.75 Å for Fe^{3+} and Ti^{4+}, respectively (16, 20, 22-24). In addition, mixtures of oxides are unlikely because the amount of iron is very small. According to Wang et al., it is possible to have iron oxides with iron doping

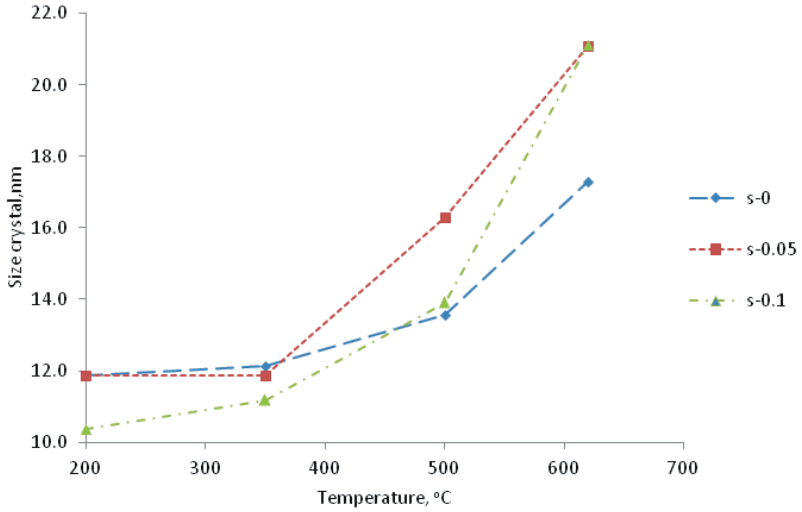

Figure 2. Crystal size of undoped TiO_2, 0.05% Fe-doped TiO_2 and 0.1% Fe-doped TiO_2, without calcination (200°C) and calcined at 350°C, 500°C and 620°C.

of 5% or more (25). Other researchers state that during the calcination process, the preadsorbed precursor (iron nitrate, for example) is decomposed, and the iron initially present at the surface diffuses into the bulk, producing a solid solution. Specimens containing up to 1% Fe are substitutional solid solutions in which Fe^{3+} is dispersed in the lattice of TiO_2, specimens with higher iron contents to accommodate any excess of iron as minute particles or small aggregates of iron oxides (hematite) and or mixed oxides at the surface of the solid solution particles (26). The brookite phase could not be observed by XRD; this phase has been reported in acidic conditions with a pH between 1.8 and 3.6 (27). In addition, it is possible that the main (101) diffraction peak of anatase at $2\theta = 25.28°$ overlaps with the (120) and (111) peaks of brookite at $2\theta = 25.34°$ and 25.69°, respectively (28).

The fraction of the rutile phase in the sample 0.05% Fe-doped, calcined at 620°C, was 17%, which could be due to the presence of iron in the material, according with researchers that report that incorporation of a metal cation favors the formation of rutile (29). This fact was attributed to particles of segregated iron oxides (M_2O_n) that could act as rutilization centers or the remaining M species in the titanium dioxide crystal structure, which have a positive influence on promotion of rutile formation (29).

It is also observed that as the calcination temperatures rises, the crystallinity increases, as well. This effect can be seen in the increase in the height of the diffraction peaks. On the contrary, the rise in the amount of iron had the opposite effect because crystallinity slightly decreased due to the distortion of the lattice (20, 30). The crystal size was estimated using the Scherrer equation, and the results are presented in Figure 2. We can see that the sintering process caused an increase in the crystal size and therefore a decrease in the surface area. Additionally, we observed an effect caused by the amount of dopant; greater amounts of iron added to the synthesis led to smaller crystal sizes (27, 30-31). This effect was minor compared to the increase in the calcination temperature. This finding is consistent with the XRD results because the crystal size increment is associated with higher crystallinity.

Raman Spectroscopy

Figure 3 shows the samples s-0.05-620 and s-0.1-620. The 0.1% Fe-doped TiO_2 sample has all the vibrational modes of anatase: 143 cm^{-1} (Eg, very intense), 196 cm^{-1} (Eg, weak), 396 cm^{-1} (B_{1g}, medium), 516 cm^{-1} ($A_{1g} + B_{1g}$, medium) and 639 cm^{-1} (Eg, medium) (32), which confirmed that the XRD results were related to the presence of anatase. This sample shows two other Raman peaks at 320 cm^{-1} and 366 cm^{-1} (close to the B1g peak of the anatase) corresponding to (B_1g, weak) and (B_2g, weak), respectively. These peaks are assigned to the TiO_2 brookite phase (33), although this phase could not be observed by XRD because of the overlapping of the peaks and its low amount. These phase compositions may be due to the amount of iron doped, which in addition to leading to an early rutilization can also influence the generation of the brookite phase, which could have been promoted instead of the rutile phase when greater amounts of iron are incorporated. All the vibrational modes of anatase were also detected in the 0.05% Fe-doped TiO_2 sample. In addition, the presence of rutile was confirmed in this sample by two signals. The first signal is an Eg vibration mode at 445 cm^{-1}

Table 1. Raman vibrational modes for 0.05% Fe-doped TiO_2 and 0.1% Fe-doped TiO_2, calcined at 620°C.

Synthesis	Band Eg (v_6)	B_{1g} (v_4)	Eg (A_{1g} (v_3) +B_{1g} (v_2)	Eg (v_1)	Eg (v_5)
s-0.1-200	141.35	396.12	514.67	637.37	194.38
s-0.1-500	141.35	394.04	514.67	636.33	194.38
s-0.1-620	140.31	394.04	512.59	638.37	193.34
s-0.1-620 Brookite bands	320.42	365.61 (B_{2g})			
s-0.05-620	140.31	396.04	512.59	637.37	193.34
s-0.05-620 Rutile Bands	445 **Eg**		611.38 (A_{1g})		

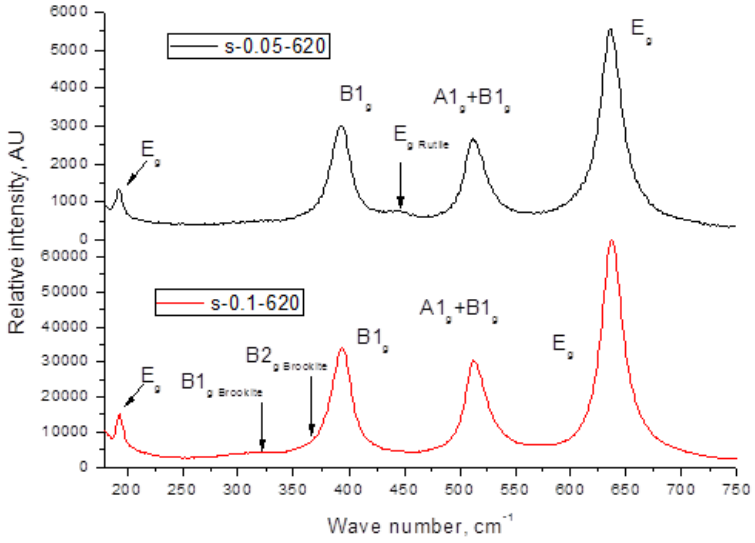

Figure 3. Raman spectra for 0.05% Fe-doped TiO_2 and 0.1% Fe-doped TiO_2, calcined at 620°C.

with a very small peak. The second is the A1g mode with a value of 638.11 cm^{-1}, which is superimposed over the Eg peak of the anatase.

Table 1 shows some vibrational modes for the 0.1% and 0.05% Fe-doped TiO_2 samples. There is a slight movement of Eg (v6) towards lower values with increasing calcination temperature from 500°C upwards, which is mainly attributable to the effect of crystal growth (34-36). This behavior states that there are small shifts in the bands with increments in the calcination temperature, i.e., the E_g (v1) band increased slightly from 637.37 cm^{-1} to 638.37 cm^{-1}; on the other hand, B_{1g} (v4) decreased from 396.12 cm^{-1} to 394.04 cm^{-1}.

Surface Area

In Figure 4, the BET surface areas of the synthesized materials are shown and two effects can be observed. The first effect shows that the surface area decreases significantly as the calcination temperature of the samples increases. The changes occur between 200°C and 350°C; and also between the 500°C and 620°C. Those changes are most likely due to size particle increment. The other effect is related to the amount of iron in the synthesis for the

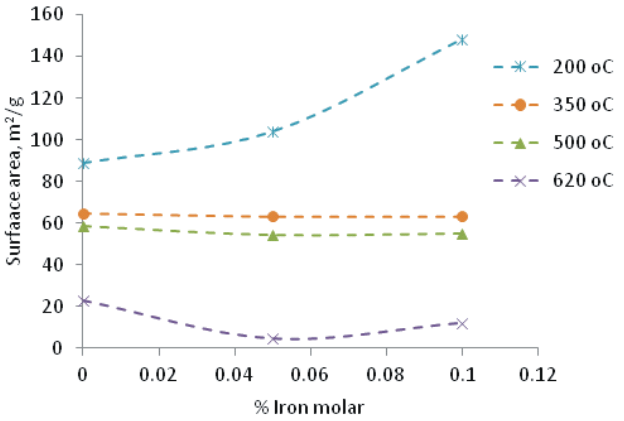

Figure 4. Surface areas of undoped TiO_2, 0.05% Fe-doped TiO_2 and 0.1% Fe-doped TiO_2, without calcination (200°C) and calcined at 350 °C, 500 °C and 620°C.

non-calcinated sample (200°C), which has the effect of increasing the surface area. In addition, the sample s-0.05- 620, has a very low surface area, (less than 5 m^2/g). This sudden drop in surface area is associated primarily with the presence of rutile in this sample (25), as well as with the synthesis method. When these results are compared with those of the crystal sizes in Figure 2, a correlation between the increase in crystal

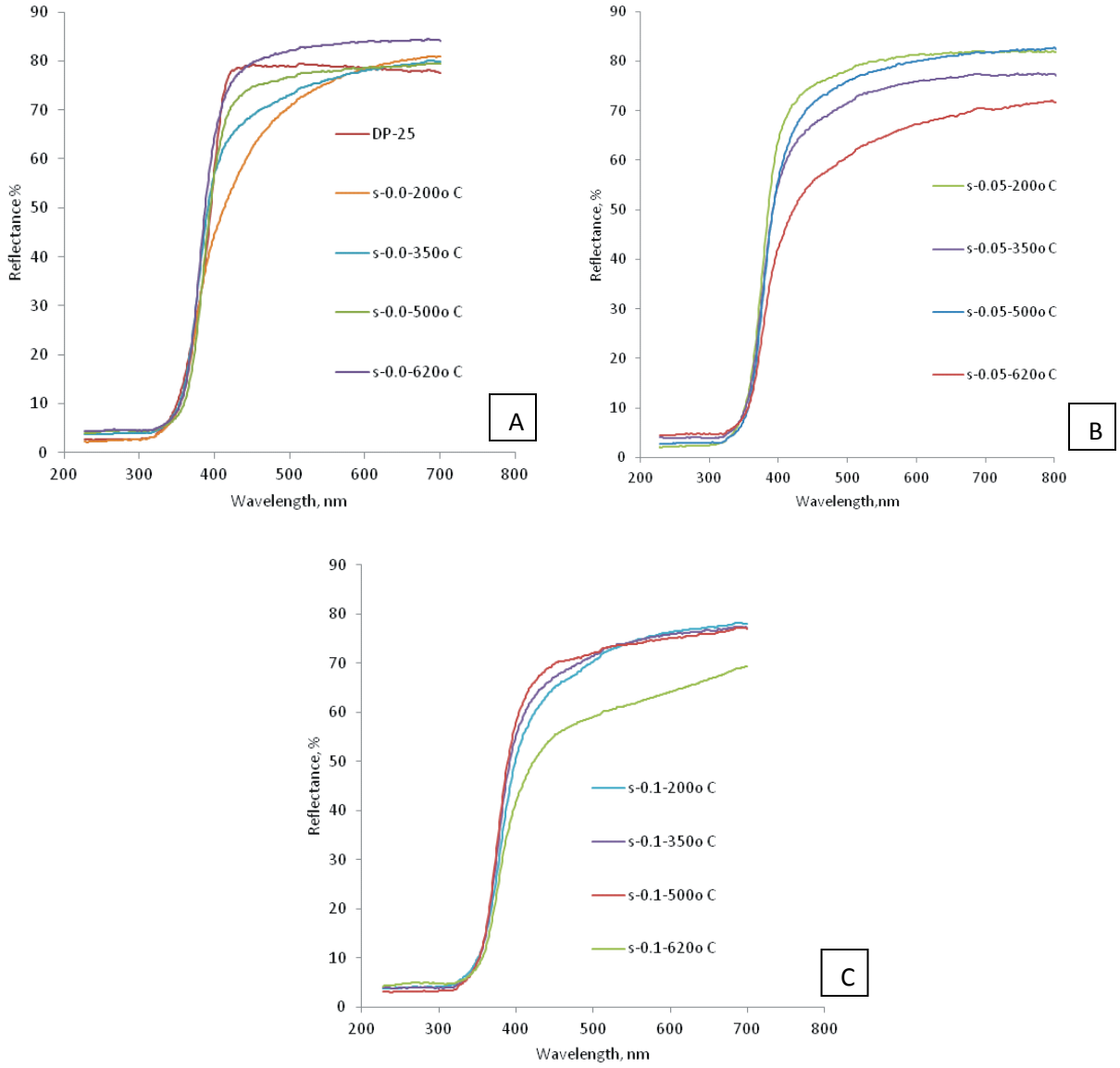

Figure 5. UV-visible Diffuse reflectance spectra of undoped TiO_2 (A), 0.05% Fe-doped TiO_2 (B) and 0.1% Fe-doped TiO_2 (C), without calcination (200°C) and calcined at 350°C, 500°C and 620°C.

size and the decrease in surface area for the effect of increasing calcination temperature is observed (31). A small increment is also observed in the surface area for the 0.1% Fe-doped TiO_2, calcined at 620 °C, which is likely attributed to the presence of brookite in the sample.

X-ray Fluorescence XRF

The amount of iron for the 0.05% Fe-doped TiO_2 and 0.1% Fe-doped TiO_2 samples was determined by XRF analysis in 0.024% and 0.042%, mass basis, respectively. These percentages indicated that we could incorporate approximately 40 % of the iron in the synthesis. Other researchers have reported that samples with higher iron content (i.e., higher than 1.2%) have a loss of iron of approximately 20–25% related to the amount added in the synthesis process (37). Adan et al., (2007) (32) reported a loss of iron of about 25%-50%. These differences can be attributed to the synthesis methods used.

Diffuse Reflectance Spectra, DRS

Figure 5 shows UV-visible spectra for the undoped TiO_2 sample (A), the 0.05% Fe-doped TiO_2 sample (B) and the 0.1% Fe-doped TiO_2 sample (C); we included the Degussa P-25 for comparison. For the undoped samples, a shift towards the ultraviolet spectrum is observed in samples with higher calcination temperatures, which is mainly due to the increase in the crystallinity, consistent with the XRD results. In contrast, this behavior changes markedly with the addition of 0.05% and 0.1% of iron. The spectra are

shifted toward the visible spectrum, especially for the samples calcined at 620°C. This effect might also be associated with the presence of some rutile or brookite in the samples s-0.05-620 and s-0.1-620, respectively.

The shift to the visible spectrum is attributed to charge transitions (or excitation) between the 3d electrons of the Fe^{3+} ion and the TiO_2 conduction band (25, 27, 38-39). We estimated the indirect band gap for the samples, as shown in Table 2. The band gap was obtained by making a Kubelka –Munk, function $[F(R)E]^{1/2}$ versus absorbed energy. We made an extrapolation in y=0 though a straight line (40):

$$F(R) = \frac{(1-R)^2}{2R} \qquad \text{Eq. 2}$$

On the x axis, the energy function is graphed thus

$$E = \frac{hC}{\lambda} \qquad \text{Eq. 3}$$

Table 2 shows slight differences with respect to band gap values. However, samples s-0.05-620 and s-0.1-620 showed small values in which lambda was higher than 400 nm. This fact confirms the likelihood that they have visible activity. In addition sample s-0.1-500, has a very high band gap value, which is consistent with having very good UV photocatalytic activity.

UV Photocatalytic Activity

Figure 6 shows that the samples with higher efficiency in the degradation of Cibacron Yellow LS-R were calcined at 500°C, regardless of the amount of iron added. The s-0.05-620 and s-0.1-620 had the worst bleaching percentages due to the loss of surface area. These results can be attributed to the presence of rutile or brookite in the samples, which are phases with lower UV photocatalytic performance compared to anatase. In addition, we observed that the material which presented brookite phase led to greater degradation of Cibacron Yellow LS-R than the material which presented rutile phase, perhaps due to a higher UV photoactivity or a larger surface area. It is envisaged that the better optimum concentration for iron doping is 0.1% because the samples prepared this iron concentration and treated at temperatures between 200°C and 500°C showed the largest percentage of discoloration. The highest percentage of discoloration in the UV radiation was reached with the s-0.1-500 sample. That's means that 0.1% of iron is an optimum concentration for doping. Then, for treatment temperatures between 200°C-500, the low values of iron doping contribute to decreasing electron-hole recombination (37).

Table 2. Band gap estimation of undoped TiO_2, 0.05% Fe-doped TiO_2 and 0.1% Fe-doped TiO_2, without calcination (200°C) and calcined at 350°C, 500°C and 620°C.

sample	Band gap, eV
s-00-200°C	3.09
s-0.05-200°C	3.11
s-0.1-200°C	3.03
s-00-350°C	3.04
s-0.05-350°C	3.10
s-0.1-350°C	3.10
s-00-500°C	3.00
s-0.05-500°C	3.10
s-0.1-500°C	3.12
s-00-620°C	3.08
s-0.05-620°C	3.01
s-0.1-620°C	2.97
DP-25	3.08

For this synthesis method, the 0.05% and 0.1% of iron doping improved the photocatalytic activity compared with the undoped samples. These synthesized samples had similar removal efficiencies to the commercial photocatalyst, DP-25. As seen in Figure 5B, it can be seen that there is coherence between absorption and bleaching activity exhibited by the samples s-0.05. The sample s-0.05-200 had the higher UV absorption and had the highest percentage of discoloration in the UV radiation (72%), the sample s-0.05-500 had the second highest UV absorption and had the second higher percentage of discoloration (71%). Sample s-0.05-350 showed the lowest percentage of discoloration (50%), apart from the sample s-0.05-620.

The decrease in color is associated with the breaking of the bonds in the azo chromophores. The subsequent step is hydroxylation in aromatic rings. This mechanism is due to the production of sulfonated aromatic amines, carboxylic acids, quinones (41), and also sulfates, nitrates and fluorides.

Photocatalytic Activity under Visible-light Radiation

Figure 7 shows the results of degradation under visible-light radiation for phenol and Cibacron Yellow LS-R. The degradation of phenol reaches almost 20% and 10% for Cibacron Yellow LS-R, for the samples doped with 0.05% and 0.1% of iron and calcined at 620°C respectively. The other materials were evaluated, but none showed activity in the visible spectrum. This effect can be explained by the results of the diffuse reflectance spectra. These samples were the only two that shifted toward the visible spectrum. Gracia et al., (2004) (29) stated that the condition of displacement in the visible spectrum does not ensure that degradation

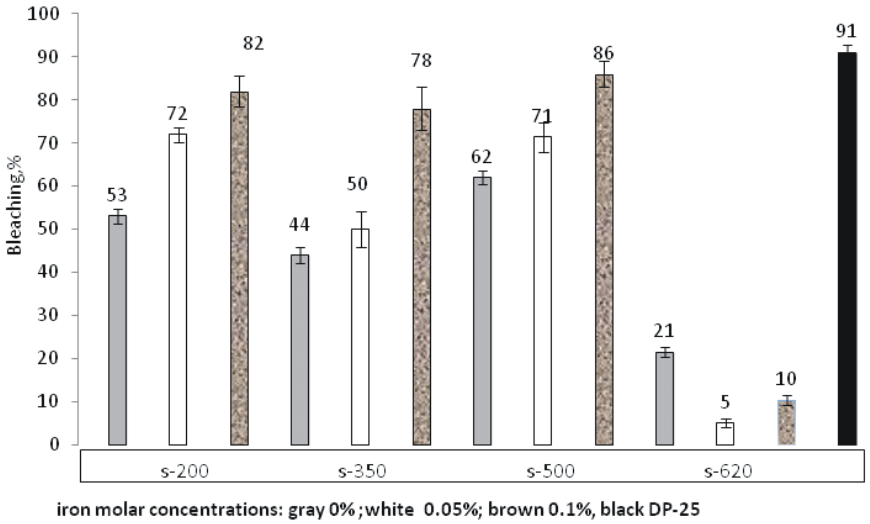

Figure 6. UV Photocatalytic activities of the undoped and doped synthesized samples and TiO_2 DP 25 in the degradation of Cibacron Yellow LS-R.

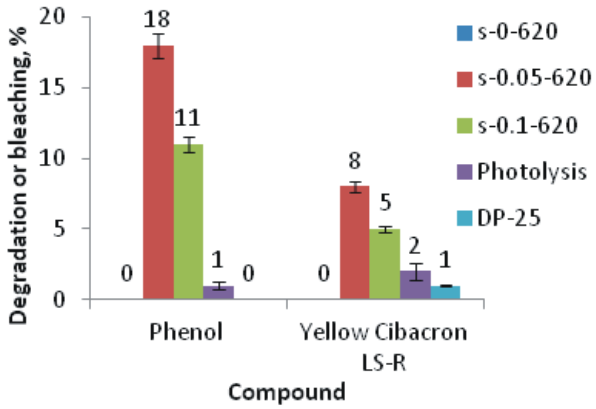

Figure 7. Photocatalytic activities in the visible spectra for s-0-620, s-0.05-620, s-0.1-620 and TiO_2 DP-25 in the degradation of the Cibacron Yellow LS-R and phenol.

will occur in this spectrum. In this case, the additional conditions seems to be the effects of the calcination temperature and the presence of rutile in the sample. This result is consistent with that presented by Wang and coworkers (2010) (11), who attribute the activity in the visible spectrum to the presence of rutile. According to these researchers, at 600°C the rutile phase forms a layer on the surface of the anatase particles. These two phases create a very thin interface or transition state. Due to the high band gap of anatase, the rutile phase can be more easily excited by visible light, and photogenerated electrons are then transferred from the valence band to the conduction band of the rutile layer. Thus, the electron-hole pair occurs synchronously (11). For the visible continuous irradiation, the photogenerated electrons are inserted into the fine interphase and enter in the conduction band for the anatase phase of TiO_2. Moreover, due to the presence of Fe^{3+} ions, the generated photoelectrons are captured immediately and the ions Fe^{3+} are then reduced to Fe^{2+} ions. Therefore, the photogenerated electrons and holes are separated completely (11). Phenol had higher photodegradated than the Yellow Cibacron LS-R under visible radiation, perhaps due to the lower molecular weight and its simple molecular structure. In contrast, Cibacron Yellow LS-R has less photodegradation perhaps due it has a higher molecular weight and complexity in its molecular structure because of the heterocyclic rings. Degussa P-25 TiO_2, which has two phases, namely, anatase (80%) and rutile (20%), exhibits a negligible visible photocatalytic activity compared with the synthesized photocatalyst (s-0.05-620), which also comprises anatase and rutile in similar proportions. This photoactivity difference is attributed to the presence of iron in the sample, which promotes the shift to the visible spectrum and partial rutilization.

Conclusions

The samples doped with 0.05% and 0.1% of iron and calcined at 620°C achieved the shift to the visible spectrum. Their photocatalytic activity obtained under visible-light irradiation was attributed to the calcination temperature, the displacement of the visible spectra and the presence of rutile, which was only detected by DRX in the sample doped with 0.05% of iron. Rutile appears due to the presence of segregated iron oxide particles (M_2O_n) that could act as rutilization centers. The sample doped with 0.1% of iron contains brookite and it is also likely that this sample contained a small amount of rutile that could not be detected by XRD or Raman spectroscopy.

Increasing the calcination temperature of the doped samples resulted in an increase in the sample crystallinity, an increase in particle size, a decrease in the surface area and the production of rutile at 620°C observed for the 0.05% Fe-TiO_2 sample. The photocatalytic activity in the UV spectrum was improved for samples that contained only anatase and were treated to a temperature between 200°C and 500°C. However, samples calcined at 620°C have a significantly decreased UV photocatalytic activity due to loss of their surface area and perhaps the presence of other phases.

The sample doped with 0.1% of iron showed the best performance in UV photocatalytic activity, independent of the calcination temperature, when 100% anatase was present.

Acknowledgements

We are grateful to the Estrategia de Sostenibilidad 2013-2014 de la Universidad de Antioquia (Colombia) for financial support and to COLCIENCIAS for the scholarship funding of the PhD studies of Ximena Vargas.

References

(1) Delpla, I.; Jung, A.V.; Baures, E.; Clement, M.; Thomas, O. *Environ Inter* **2009**, *35*, 1225-1233.

(2) Theron, J.; Walker, J.A.; Cloete, T.E. *Crit Rev Microbiol* **2008**, *34*, 43-69.

(3) Ohtani, B. *J. Photochem Photobiol C: Photochem Rev*. **2010**, *11*, 157-178.

(4) Gaya, U.I; Abdullah, A.H. *J Photochem Photobiol C: Photochem Rev* **2008**, *9*, 1-12.

(5) Rajeshwar, K.; Osugi, M.E.; Chanmanee, W.; Chenthamarakshan, C.R.; Zanoni, M.V.B.; Kajitvichyanukul, P.; Krishnan-Ayer, R. *J Photochem Photobiol. C: Photochem Rev* **2008**, *9*, 171-192.

(6) Lhomme, L.; Brosillon, S.; Wolbert, D. *Chemosphere* **2008**, *70*, 381-386.

(7) Jing, J.; Liu, M.; Colvin, V.L.; Li, W.; Yu, W.W. *J Mol Catal. A: Chem* **2011**, *351*, 17- 28.

(8) Colmenares, J.C.; Aramendia, M.A.; Marinas, A.; Marinas, J.A.; Urbano, F. *J Appl Catal A* **2006**, *306*, 120-127.

(9) Othman, S.H.; Rashid, S.A.; Ghazi,T.I.; Abdulla, N. *J Nanomater* **2011**, 1-8.

(10) Feng, H.; Zhang, M.H.; Yu, L.E. *Appl Catal A* **2012**, *413- 414*, 238-244.

(11) Wang, J.; Li, R.; Zhang, L.; Xie, Y.; Jiang, Z.; Xu, R.; Xing, Z.; Zhang, X. *Russ J Inor Chem* **2010**, *55*, 692-699.

(12) Hung, W.; Fu, S.; Tseng, J.; Chu, H.; Ko, T. *Chemosphere* **2007**, *66*, 2142-2151.

(13) Naeem, K.; Ouyang, F. *Physica B* **2010**, *405*, 221-226.

(14) Popa, M. ; Diamandescu, L. ; Vasiliu, F. ; Teodorescu, CM. ;Cosoveanu, V. ;Baia, M. ; Feder, M. ; Baia, L. ; Danciu, V. *J Mater Sci* **2009**, *44*, 358-364.

(15) Xin, B.; Ren, Z.; Wang, P.; Liu, J.; Jing, L.; Fu, H. *Appl Surf Sci* **2007**, *253*, 4390-4395.

(16) Zhou, M.; Yu, J.; Cheng, B.; Yu, H. *Mater Chem Phys* **2005**, *93*, 159-163.

(17) Zhou, M.; Yu, J.; Cheng, B. *J Hazard Mater* **2006**, *B137*, 1838-1847.

(18) Vargas, X.; Tauchert, E.; Marin, J.M.; Restrepo, G.; Dillert, R.; Bahnemann, D. *J Photochem Photobiol A: Chem* **2012**, *243*, 17-22.

(19) Kositzi, M.; Poulios, I.; Samara, K.; Tsatsaroni, E.; Darakas, E. *J Hazard Mater* **2007**, *146*, 680-685.

(20) Asilturk, M.; Sayılkana, F.; Arpac, E. *J Photochem Photobiol A: Chem* **2009**, *203*, 64-71.

(21) Hirano, M.; Joji, T.; Inagaki, H.; Iwata, H. *J Amer Cer Soc* **2004**, *87*, 35-41.

(22) Araña, J.; González, O.; Rodríguez, J.M.; Herrera, J.A.; Garriga, C.; Caboa, I.; Pérez, J.; Hidalgo, M.C.; Navío, J.A. *J Mol Catal A: Chem* **2003**, *197*, 157-171.

(23) Li, J.; Xu, J.; Dai, W.; Li, H.; Fan, K. *Appl Catal B: Environ* **2009**, *85*, 162-170.

(24) Wang, C.; Bottcher, C.; Bahnemann, D.; Dohrmann, J. *J Mater Chem* **2003**, *13*, 2322-2329.

(25) Wang, J.A.; Limas-Ballesteros, R.; López, T.; Moreno, A.; Gómez, R.; Novaro, O.; Bokhimi, X. *J. Phys Chem B* **2001**, *105*, 9692-9698.

(26) Litter, M.I.; Navio, J.A. *J. Photochem Photobiol A: Chem* **1996**, *98*, 171-181.

(27) Wang, M.C.; Lin, H.J.; Yang, T.S. *J Alloy Compd* **2009**, *473*, 394-400.

(28) Di Paola, A.; Bellardita, M.; Palmisano, L. *Catalysts* **2013**, *3*, 36-73.

(29) Gracia, F.; Holgado, J.P.; Yubero, F.; Gonzalez-Elipe, A.R. *J Phys Chem B* **2004**, *108*, 17466-17476.

(30) Lee, H.Y.; Lan, W.L.; Tseng, T.Y.; Hsu, D.; Chang, Y.M.; Lin, J.G. *Nanotech* **2009**, *20*, 315702-315707.

(31) Sijakovic, N.; Gotic, M.; Ivanda, M.; Popovic, S. *J Sol Gel Sci Tech* **2004**, *30*, 5-19.

(32) Adán, C.; Bahamonde, A.; Fernández-García, M.; Martınez-Arias, A. *Appl Catal B: Environ* **2007**, *72*, 11-17.

(33) Tompsett, G.A.; Bowmaker, G.A.; Cooney, R.P.; Metson, J.B.; Rodgers, K.A.; Seakins, J.M. *J Raman Spectrosc* **1995**, *26*, 57-62.

(34) Choi, H.; Jung, Y.; Kim, S. *Vib Spectrosc* **2005**, *37*, 33-38

(35) Mahdjoub, N.; Allen, N.; Kelly, P.; Vishnyakov, V. *J Photochem Photobiol A: Chem* **2010**, *211*, 59-64.

(36) Šćepanović, M.J.; Grujić-Brojčin, M.; Dohčević-Mitrović, Z.D.; Popović, Z.V. *Sci Sinter* **2009**, *41*, 67-73.

(37) Ambrus, Z.; Balazs, N.; Alapi, T.; Wittmann, G,; Sipos, P.; Dombi, A.; Mogyorosi, K. *Appl Catal B: Environ* **2008**, *81*, 27-37.

(38) Wang, Y.; Cheng, H.; Hao, Y.; Ma, J.; Li, W.; Cai, S. *J of Mater Sci* **1999**, *34*, 3721-3729.

(39) Zhu, J.; Zheng, W.; He, B.; Zhang, J.; Anpo, M. *J Mol Catal A: Chem* **2004**, *216*, 35-43.

(40) Ismail, A.; Bahnemann, D.; Robben, L.; Yarovyi, V.; Wark, M. *Chem Mater* **2010**, *22*, 108-116.

(41) Torrades, F.; García-Montaño, J.; García-Hortal, J.A.; Núñez, L.; Domènech, X.; Peral, J. *Color Technol* **2004**, *120*, 188-194.

Received for review September 3, 2014. Revised manuscript received December 22, 2014. Accepted December 27, 2014.